UAV-Assisted Communications with RIS: A Shadowing-based Stochastic Analysis

Petros S. Bithas, *Senior Member, IEEE*, George A. Ropokis, George K. Karagiannidis, *Fellow, IEEE*, and Hector E. Nistazakis

***Abstract*—We study and analyze the performance of a wireless communication system that is based on the use of airborne Reconfigurable Intelligent Surfaces, i.e., surfaces mounted on an Unmanned Aerial Vehicle (UAV). To this end, we perform a stochastic analysis that allows us to study a very wide variety of realistic channel conditions, including environments characterized by combined small-scale and large-scale fading and potential spatial correlation in shadowing. For this generic channel model, we derive closed-form expressions for the outage probability and the ergodic capacity, and also investigate the analytical calculation of the average energy efficiency. The presented results allow us, for the first time, to study the impact of different shadowing conditions, including correlation effects, in aerial communications systems that are also supported by reconfigurable intelligent surfaces. Finally, the performance of the considered system is also compared with that of decode-and-forward relaying, highlighting the advantages of combining reconfigurable intelligent surfaces with UAV-assisted communication technologies in composite fading environments.**

***Index Terms*—Correlation, energy efficiency, reconfigurable intelligent surfaces, shadowing, unmanned aerial vehicles (UAVs).**

I. Introduction

RECONFIGURABLE Intelligent Surfaces (RISs), i.e., man-made surfaces, composed by electronically tunable elements, are a promising technology for shaping favorable propagation conditions by controlling the functionality of each one of the RIS's elements [1]. Key RIS technologies enabling this concept include dynamic reflecting arrays, tunable metasurfaces, and liquid crystal surfaces, which offer different ways for controlling the key characteristics of the reradiated electromagnetic waves, such as the phase [2], [3].

Besides RISs, another approach to obtain favorable propagation conditions and improve coverage, is to use Unmanned Aerial Vehicles (UAVs) for communication purposes, which can increase the probability of Line-of-Sight (LoS). In addition, the combination of UAVs and RISs can be a very promising step forward to provide highly reliable, high rate communications, and thus enabling the 6th generation communication networks use-cases and applications [4], [5]. Therefore, the joint exploitation of these two technologies is currently being investigated. In more detail, in [6], the effects of small-scale fading on airborne RIS-assisted communications (i.e., communications achieved with the aid of RISs mounted on UAVs) are studied. The presence of $\kappa-\mu$ distributed fading is considered, and the performance of airborne RIS-assisted communication was investigated, using various criteria, including the Outage Probability (OP), the Bit Error Rate (BER), and the ergodic capacity. The same performance metrics are also studied in [7] and used to investigate the problem of determining the optimal altitude of RIS-equipped UAV. In [8], the use of Non-Orthogonal Multiple Access (NOMA) in airborne RIS-assisted communication systems is studied, and a decaying deep Q-network algorithm is proposed to minimize the energy consumption. In [9], the use of RIS-supported UAVs in high-mobility communications scenarios was investigated, and it was found that even low-complexity RIS configurations can provide significant performance improvements over non-RIS based designs. In [10], the impact of interference has been analytically investigated in airborne RIS-assisted inter-vehicular communication scenario. Finally, in [11], an integrated Free Space Optical-Radio Frequency (FSO-RF) satellite-aerial-ground network has been studied, in which the UAV is equipped with RIS. The results presented in [11] show that RIS equipped UAVs can achieve considerable communication performance improvements in turbulent fading channels.

With shadowing being another important limiting factor for communications systems, the effects of shadowing on airborne RIS-assisted systems need to be investigated. In this direction, some initial performance results have recently been published in [12], [13]. In particular, in [12], assuming a composite fading environment modeled by the Nakagami-inverse gamma distribution, approximate, but rather complicated, expressions were derived for the OP, while a deep neural network was also proposed to predict the OP. In [13], the results of [12] were generalized to a composite shadowing/small scale fading Multiple-Input Multiple-Output (MIMO) communication scenario, modeled by the generalized-K distribution. More specifically, assuming independent shadowing on the channel between the source and the RIS, and the channel between the RIS and the destination, the performance of this communication system in terms of OP and BER has been studied.

Although, in general, the assumption of independent shadowing is valid, in many cases, the presence of correlation in the

Manuscript received XXXX, 2023;

P. S. Bithas is with the Department of Digital Industry Technologies, National and Kapodistrian University of Athens, Athens, 15784, Greece. (e-mail: pbithas@dind.uoa.gr).

G. A. Ropokis is with CentraleSupélec, Campus Rennes, 35510, Cesson Sevigne, France and the Institute of Electronics and Telecommunication of Rennes, France (e-mail: georgios.ropokis@centralesupelec.fr).

G. K. Karagiannidis is with Department of Electrical and Computer Engineering, Aristotle University of Thessaloniki, Greece and also with Artificial Intelligence & Cyber Systems Research Center, Lebanese American University (LAU), Lebanon (e-mail: geokarag@auth.gr).

H. E. Nistazakis is with the Department of Physics, Section of Electronic Physics and Systems, National and Kapodistrian University of Athens, Athens, 15784, Greece. (e-mail: enistaz@phys.uoa.gr).

Digital Object Identifier 10.1109/XXXXXXXXXXXXXXX

shadowing cannot be ignored. This correlation is introduced by the inherent characteristics of UAV flying environment [14] as well as the small distances among the RIS elements in conjunction with the large decorrelation distance of the shadowing. However, for analytical simplification purposes, the shadowing correlation is not taken into account in the previous studies. Motivated by this observation, in this paper, we develop an analytical investigation for the impact of large-scale fading in airborne-RIS enabled communications (i.e., RISs mounted on UAVs), by also considering the impact of shadowing correlation. More specifically, the contributions of the paper are as follows:

- We propose a new composite fading channel for airborne RIS-assisted communications that models the presence of both small-scale fading and shadowing on the links between the source/destination and the airborne RIS. The new model is generic and also takes into account the presence of shadowing correlation.
- To analyze the statistical properties of this model, we study the stochastic characteristics of the product of two arbitrarily correlated, Inverse-Gamma (IG) Random Variables (RVs), and derive closed-form expressions for the Probability Density Function (PDF) and the Cumulative Distribution Function (CDF) of this product. To the best of our knowledge, this is the first time that a closed-form expression for the PDF and CDF of such a product is derived. We then use this result to derive expressions for the PDF and CDF of the received signal-to-noise ratio (SNR), for our model. Finally, we note that besides our investigation, products of IG RVs are often encountered in a variety of communications scenarios, e.g., in environments where double-scattering propagation conditions exist [15]. Therefore, our results can be easily applied to these scenarios as well.
- We analyze the performance of the considered system using the criteria of OP, ergodic channel capacity, and average energy efficiency.
- We also derive novel analytical expressions for the OP and ergodic capacity of benchmarks for our system that employ Full Duplex (FD) and Half Duplex (HD) cooperative protocols at the UAV, instead of an RIS. The numerical performance comparisons of all systems examined, in different composite fading scenarios, illustrate that airborne RIS-assisted communications provide superior performance, as compared to traditional cooperative techniques.

The rest of this paper is organized as follows. In Section II, the system and channel models under consideration are presented. In Section III, an approximated analysis for the statistics of the small scale fading effects is presented. In Section IV, we study the statistics of the product of correlated IG RVs, and exploit the derived results for the performance analysis of the system under consideration. In Section V, various numerical evaluated results are presented, while Section VI summarizes our conclusions.

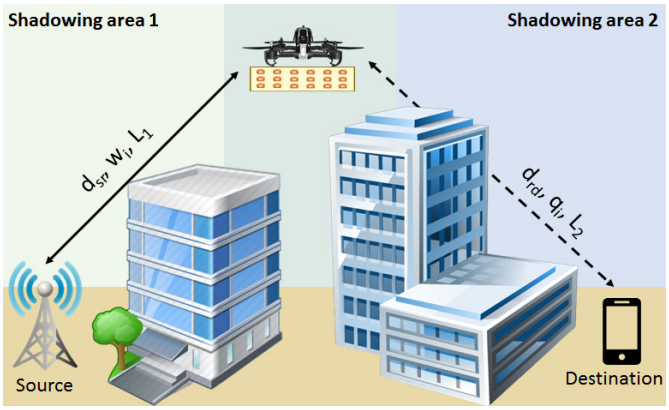

Fig. 1: System model considered.

II. System and Channel Models

A. System model

We consider a communication system in which a single-antenna source (S), communicates with a single-antenna destination (D) with the aid of an airborne RIS, which is shown in Fig. 1. By exploiting the advantages of UAV-mounted RIS networks, the communication performance is enhanced especially in Internet of Things scenarios, where time variant Quality of Services (QoS) requirements exist [16]. The airborne RIS is equipped with M reflecting elements and an RIS controller that can dynamically adjust the phase shifts applied at each RIS element. In this work, we assume that perfect Channel State Information (CSI) is available at the S, D, and the airborne RIS, resulting to ideal phase-shifting at the RIS [17]. Finally, we focus on scenarios where the S to D channel is severely attenuated due to shadowing and can be therefore ignored. As a result, communication takes place only with the help of the airborne RIS[1].

Let d_{sr} be the distance between S and the RIS, d_{rd} the distance between the RIS and D, and v the path-loss exponent of our propagation model. The signal reaching D is then expressed as

$$y = \sqrt{\frac{P_S}{d_{sr}^v d_{rd}^v}} \sum_{i=1}^{M} h_{sr,i} e^{j\theta_i} h_{rd,i} s + n, \tag{1}$$

where s denotes the unit power transmitted signal, and P_S the transmit power at S. Furthermore, the random complex coefficients $h_{sr,i} = w_i L_1 e^{j\phi_i}$ and $h_{rd,i} = q_i L_2 e^{j\varphi_i}, i = 1, \ldots, M$, model the combined shadowing and small scale fading effects on the channels from S to the i-th reflecting element of the RIS, and from the i-th reflecting element of the RIS to D, respectively. In more detail, RVs $w_i, q_i, i = 1, \ldots, M$, model the small scale fading magnitude, and $\phi_i, \varphi_i \in [0, 2\pi)$ the small scale fading phase effects, while L_1, L_2 model the shadowing random variations. The channel gain and shadowing coefficients are also depicted in Fig. 1. Finally, in (1), n

[1]Although from a theoretical perspective the combined presence of a LoS component and the RIS-aided channel would be interesting, the theoretical investigation of such a scenario within the context of UAV-aided RIS communications is very challenging, due to the path losses and delays differences, between the 2 different paths, i.e., S→D and S→RIS→D.

denotes the Additive White Gaussian Noise (AWGN), with zero mean and variance N_0.

In the above signal model, we assume that the effect of shadowing is the same for all channels between S and reflecting elements of the RIS and thus they are modeled by a single RV L_1. The reason behind this choice is the fact that shadowing effects are highly correlated for distances of the order of tenths of meters. As a result, since the RIS reflecting elements are placed in much closer distances, we can expect that the effects of shadowing for all channels between S and the RIS elements are identical. Similarly, we use the same assumption for the channels from the RIS to D, and also model shadowing for all these channels using a single RV L_2. Finally, we note that these two assumptions of identical shadowing on all S to RIS channels (or RIS to D channels), is aligned with the common assumption of identical shadowing, which is commonly adopted when studying multi-antenna systems [18], [19].

From (1), the SNR at D is written as

$$\gamma = \frac{P_S}{N_0 d_{sr}^v d_{rd}^v} \left| \sum_{i=i}^{M} w_i L_1 q_i L_2 e^{j(\theta_i - \phi_i - \varphi_i)} \right|^2, \tag{2}$$

and it is maximized if the RIS selects phase shifts θ_i to be equal to $\theta_i = \phi_i + \varphi_i$. The SNR is then written as

$$\gamma = \frac{SNR_T}{d_{sr}^v d_{rd}^v} \left(\sum_{i=i}^{M} w_i q_i \right)^2 L_1 L_2 = \frac{SNR_T}{d_{sr}^v d_{rd}^v} Z, \tag{3}$$

where Z is a RV defined as $Z \triangleq W L_1 L_2$, with $W = \left(\sum_{i=i}^{M} w_i q_i \right)^2$, while $SNR_T = P_S/N_0$ denotes the transmit SNR. From (3), it is evident that a symmetry exists at the SNR value with respect the point where the distances between S-UAV and UAV-D are equal, i.e., $d_{sr} = d_{rd}$.

B. Channel model

We model the small-scale effects on the channel between S (or D) and the airborne RIS, using the Weibull distribution. The reason for adopting this particular distribution is that it can accurately capture the fading characteristics of various scenarios, ranging from worse than Rayleigh to LoS [20], [21]. Focusing particularly on LoS scenarios, we highlight that the Weibull distribution has been proposed in [22] as an alternative channel model to the Ricean one, while in [23], a one-to-one mapping between the Weibull shaping parameter and the Ricean-K factor was proposed. On the other hand, the application of Weibull fading in non-LoS scenarios is extensive and also include UAV communications as found in [20]. As a result of the above, by employing the Weibull fading channel model, we enable a unified treatment of LoS and non-LoS airborne RIS-assisted communications scenarios. Moreover, thanks to the mathematically convenient form of the Weibull PDF, the results of this approach are analytically tractable.

We consider an independent and identically distributed (i.i.d.) small scale fading scenario, where the shape and scale parameters characterizing the Weibull distribution are the same for all fading channels. As a result, introducing RV $c \in \{w_i, q_i\}, i = 1, \ldots, M$, the PDF of c is written as

$$f_c(x) = \frac{k}{\lambda} \left(\frac{x}{\lambda} \right)^{k-1} \exp\left[- \left(\frac{x}{\lambda} \right)^k \right], \tag{4}$$

where $k > 0$ is the common (for all channels) shape parameter (related to the severity of the fading), and $\lambda > 0$ the common scale parameter.

We combine the above small scale fading model with the realistic, experimentally validated shadowing model presented in [24]. According to it, the shadow variations $L_j, j = 1, 2$, of the local mean received power at the RIS and at D, respectively, are modeled using IG distribution, having marginal PDF of the form

$$f_{L_j}(y) = \frac{1}{\Gamma(\alpha) \overline{\gamma}_j^{\alpha} y^{\alpha+1}} \exp\left(-\frac{1}{\overline{\gamma}_j y} \right), \; j = 1, 2, \tag{5}$$

where $\alpha > 1$ is the shaping parameter of the distribution, which controls the severity of the shadowing, $\overline{\gamma}_j$ is the corresponding scaling parameter of the L_j-th RV, and $\Gamma(\cdot)$ is the gamma function [25, eq. (8.310/1)].

While in the case of independent shadowing on the S to RIS and the RIS to D channels, the marginal PDFs $f_{L_j}(\cdot), j = 1, 2$, suffice in order to model our system, in several cases, shadowing effects on these two channels are expected to be correlated [26], [27]. This is particularly likely to happen especially when the distance between S and D is small. In such a scenario, the joint statistics of the two RVs L_1 and L_2 that model the correlated shadowing are captured by the bivariate IG PDF given by [28]

$$\begin{aligned} f_{L_1,L_2}(x,y) = & \frac{\rho^{\frac{1-\alpha}{2}}}{\Gamma(\alpha)(1-\rho)\left(\overline{\gamma}_1 \overline{\gamma}_2\right)^{\frac{\alpha+1}{2}} (xy)^{\frac{\alpha+3}{2}}} \\ & \times \exp\left[-\frac{1/(\overline{\gamma}_2 y) + 1/(\overline{\gamma}_1 x)}{(1-\rho)} \right] I_{\alpha-1}\left[\frac{2\sqrt{\rho}/(1-\rho)}{(\overline{\gamma}_1 \overline{\gamma}_2 xy)^{\frac{1}{2}}} \right], \end{aligned} \tag{6}$$

where ρ denotes the correlation coefficient between L_1, L_2, and $I_v(\cdot)$ denotes the modified Bessel function of the first kind and order v [25, eq. (8.406/1)].

Having described large and small scale fading statistics, in the following sections, we present our approach for accurately modeling the statistical behavior of the SNR in (3). To this end, we first discuss our methodology for approximating the PDF of W.

III. A Highly Accurate Statistical Model for W

In order to investigate the statistics of the SNR in (3), an exact expression for the PDF of the RV $W = \left(\sum_{i=i}^{M} w_i q_i \right)^2$ is required. However, deriving a convenient closed-form expression for $f_W(x)$ (or $F_W(x)$) is extremely cumbersome and no related results have been reported in the open technical literature. To overcome this difficulty, we propose an alternative approach, which is based on approximating the target PDF $f_W(x)$ by a tractable parametric PDF and selecting the parameters of this PDF such as to achieve a close fit to the target PDF. To this end, we follow the Method of Moments (MoM), described in the following subsection.

A. Using MoM to closely approximate the PDF of the SNR

When the MoM is used in order to approximate a target PDF, we start with a parametric fitting distribution, and select its parameter values such that selected moments of the target PDF match the corresponding moments of the fitting distribution. Within the wireless communications literature, the MoM has been widely used in order to approximate PDFs whose expression is difficult to be found. Indicatively, from the recent literature, we mention the work in [29], where the authors employ the MoM for fitting a Gamma distribution, which is characterized by an analytically more convenient PDF expression as compared to the generalized-K distribution.

In this work, we consider applying the MoM such as to approximate the PDF of W. As a fitting/approximating distribution, we select the Gamma distribution with PDF

$$\tilde{f}_W(x) = \frac{1}{\theta^\beta \Gamma(\beta)} x^{\beta-1} \exp\left(-\frac{x}{\theta}\right), \tag{7}$$

where β and θ are the shape and scale parameters of the Gamma distribution, respectively. The reason for choosing the Gamma distribution is the fact that it is a well studied one, it has simple stochastic metrics and thus allows for deriving closed-form expressions for the performance analysis purposes. Moreover, as it will become evident in later parts of our analysis, it allows for obtaining very close approximations for the true PDF and CDF of W.

By matching the first two moments μ_1 and μ_2 of W to the first two moments of $\tilde{f}_W(x)$ in (7), we can easily obtain the following estimators for β and θ [30]

$$\beta = \frac{\mathbb{E}[W]^2}{\mathrm{Var}[\mathrm{W}]} = \frac{\mu_1^2}{\mu_2 - \mu_1^2}, \quad \text{and} \quad \theta = \frac{\mathrm{Var}[\mathrm{W}]}{\mathbb{E}[W]} = \frac{\mu_2 - \mu_1^2}{\mu_1}, \tag{8}$$

where $\mathbb{E}[\cdot]$ denotes the expectation operator and $\mathrm{Var}[\cdot]$ denotes the variance. Since this process, requires the calculation of μ_1 and μ_2, we hereby express these two moments as

$$\begin{aligned} \mu_1 &= \sum_{i=1}^{M} \mathbb{E}[w_i]\mathbb{E}[q_i], \\ \mu_2 &= \sum_{i=1}^{M} \mathbb{E}\left[w_i^2\right] \mathbb{E}\left[q_i^2\right] \\ &\quad + 2\sum_{i=1}^{M} \sum_{j=i+1}^{M} \mathbb{E}\left[w_i\right] \mathbb{E}\left[q_i\right] \mathbb{E}\left[w_j\right] \mathbb{E}\left[q_j\right], \end{aligned} \tag{9}$$

where $\mathbb{E}[w_i^n] = \mathbb{E}[q_i^n] = \lambda^n \Gamma(1 + n/k)$ is the n-th moment of the Weibull RVs [23]. For obtaining (9), the uncorrelatedness property of RVs has been adopted [31, p. 211] as well as the multinomial identity [32, eq. (24.1.2)].

In order to assess the performance of the MoM for our channel model, in Fig. 2, we compare the empirical CDF of W, i.e., $F_W(x)$, with the empirical CDF of Gamma RV, i.e., $\tilde{F}_W(x)$. The results of Fig. 2 were obtained after setting the parameters of all Weibull RVs w_i, q_i, with $i = 1, \ldots M$, equal to $k = 2.5$, and $\lambda = 2$. In more detail, in Fig. 2, the empirical CDF of the sum of M double-Weibull RVs, i.e., $F_W(x)$, where $W = \left(\sum_{i=i}^{M} w_i q_i\right)^2$, is plotted for different values of M (this empirical CDF is denoted as Empirical CDF of W in Fig. 2). It is shown that the slope of the CDF is affected by M, i.e., it decreases as M increases. In the same figure, in an effort to understand how close approximation is offered by the MoM using the Gamma distribution in comparison to the Central Limit Theorem (CLT), more curves are included. More specifically, the empirical CDF of a RV following a Gamma distribution, with the first two moments given by (9), is shown (denoted as Gamma approx.) along with the empirical CDF of a Gaussian RV (with mean and variance being evaluated based on the rules of CLT), denoted as CLT approx. Moreover, in a further effort to quantify the quality of our approximation, in Fig. 2, we also provide the Kullback-Leibler (K-L) divergence values for the two considered approximations. It is noted that the distribution that fits best to the exact values is the one that minimizes the K-L distance, calculated by the simulated data set. In the table included in Fig. 2, it is shown that the K-L distance remains very small, using both approaches, with the Gamma-distribution providing always the closest approximation for all values of M. Although in Fig. 2 this is shown for $M \geq 10$, the same holds also for smaller values of M.

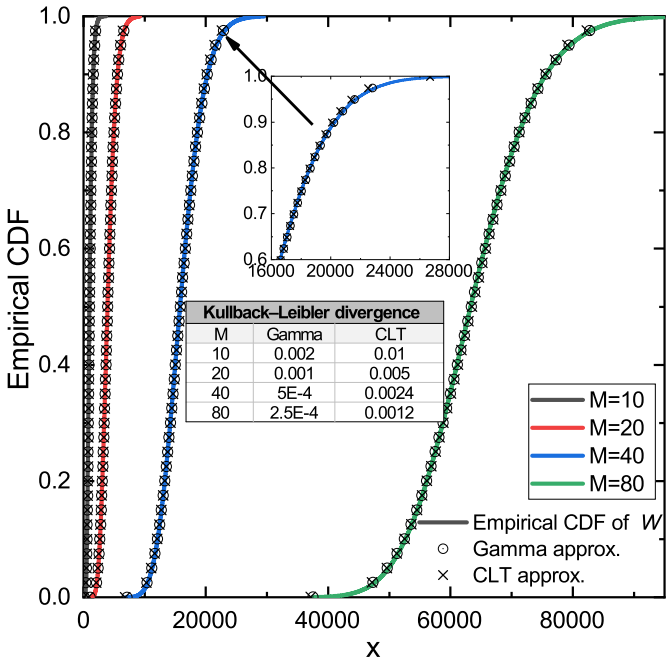

Fig. 2: Empirical CDFs comparisons.

Finalizing the presentation of the Gamma-based approximation to the PDF of W, $f_W(\cdot)$, and its comparison to the Gaussian approximation, we highlight that the Gamma distribution is described by relatively simpler expressions, as compared to the corresponding ones used for the Gaussian distribution. Therefore, IG model facilitates the analytical framework that will be presented in the next section. Taking this into account, along with the fact that the Gamma distribution is able to deliver a very close fit to empirical statistics of the PDF of W, in the rest of the manuscript, we employ this approximation for modeling the random behavior of W in airborne RIS-assisted communication scenarios.

IV. Stochastic Analysis and Performance Evaluation

In what follows, we exploit the derived accurate approximation for the PDF of W in order to derive novel approximate results for the statistics of the received SNR and analyze the performance of the considered communication system for different scenarios. To this end, recalling the definition of the SNR in (3) and the presence of the product term $L = L_1 L_2$ in this definition, we proceed by first analyzing the statistical properties of L.

A. Deriving the statistics of $L = L_1 L_2$

The PDF of the product of correlated IG RVs L_1 and L_2 can be evaluated with the aid of the following theorem.

Theorem 1. *The PDF of the RV $L \triangleq L_1 L_2$, where L_1, L_2, are correlated IG RVs following the bivariate PDF provided in* (6)*, is given by*

$$f_L(z) = \frac{2z^{-\frac{\alpha+3}{2}}/\Gamma(\alpha)}{\overline{\gamma}_1\overline{\gamma}_2\left(\overline{\gamma}_1\overline{\gamma}_2\rho\right)^{\frac{\alpha-1}{2}}} I_{\alpha-1}\left[\frac{2\sqrt{\rho}}{\sqrt{\overline{\gamma}_1\overline{\gamma}_2 z}(1-\rho)}\right] \times \frac{1}{1-\rho} K_0\left[\frac{2}{\sqrt{\overline{\gamma}_1\overline{\gamma}_2 z}(1-\rho)}\right], \tag{10}$$

where $K_v(\cdot)$ denotes the modified Bessel function of the second kind and order v [25, eq. (8.407)].

Proof: The PDF of L can be evaluated using the following formula [31, eq. (6.148)]

$$f_L(z) = \int_0^\infty \frac{1}{x} f_{L_1,L_2}\left(x, \frac{z}{x}\right) dx. \tag{11}$$

After substituting (6) in (11), employing property [25, eq. (3.471/9)], and applying some mathematical simplifications, the closed-form expression in (10) is then obtained. ∎

Furthermore, the following Lemma provides a simpler expression, for the case that L_1 and L_2 are independent RVs.

Lemma 1. *The PDF of the RV $L \triangleq L_1 L_2$, where L_1, L_2, are independent IG RVs with marginal PDFs provided in* (5)*, is given by*

$$f_L(z) = \frac{2/\Gamma(\alpha)^2}{\left(\overline{\gamma}_1\overline{\gamma}_2\right)^{\alpha} z^{\alpha+1}} K_0\left[\frac{2}{\sqrt{\overline{\gamma}_1\overline{\gamma}_2 z}}\right]. \tag{12}$$

Proof: Assuming that L_1, L_2, are independent RVs, (11) can be written in the following form $f_L(z) = \int_0^\infty \frac{1}{x} f_{L_1}(x) f_{L_2}\left(\frac{z}{x}\right) dx$. Using (5) in this definition and adopting a similar approach as the one for deriving (10), the PDF of the product of independent IG RVs given in (12) is finally obtained. ∎

Having derived the PDF of $L = L_1 L_2$, we exploit this result in order to derive the PDF of Z.

B. Deriving the statistics of Z

Starting with the general result of Theorem 1, since Z is defined as $Z = W L$, we can derive its PDF by substituting expression (7) for the PDF of W and expression (10) for the PDF of L, in the following equation [31, eq. (6.148)]

$$f_Z(x) = \int_0^\infty \frac{1}{y} \tilde{f}_W(y) f_L\left(\frac{x}{y}\right) dy. \tag{13}$$

Following that and using the infinite series representation of the $I_v(\cdot)$ [25, eq. (8.445)], as well as [25, eq. (6.643/3)], we obtain the following infinite series expression for the PDF of Z

$$f_Z(x) = \frac{1}{\Gamma(\beta)\Gamma(\alpha)\left[\bar{\gamma}_1\bar{\gamma}_2(1-\rho)\right]^{\alpha}} \sum_{i=0}^{\infty} \left(\frac{\rho}{\bar{\gamma}_1\bar{\gamma}_2(1-\rho)^2}\right)^i \times \frac{\theta^{i+\alpha}\Gamma(\beta+i+\alpha)^2}{x^{i+\alpha+1}\Gamma(\alpha+i)i!} U\left(\beta+i+\alpha, 1, \frac{\theta/x}{\bar{\gamma}_1\bar{\gamma}_2(1-\rho)^2}\right), \tag{14}$$

where $U(\cdot,\cdot,\cdot)$ denotes the confluent hypergeometric function [25, eq. (9.210/2)].

Based on (14), an expression for the CDF of Z can be also found. To this end, we start by using the Meijer's G-function representation of the confluent hypergeometric function and integrating term by term (14). Following such an approach and exploiting property [33, eq. (26)], the following exact expression for the CDF of Z is found

$$F_Z(x) = \sum_{i=0}^{\infty} \frac{1}{\Gamma(\beta)} \frac{(1-\rho)^{\alpha}}{\Gamma(\alpha)} \frac{\rho^i}{\Gamma(\alpha+i)i!} \times G_{2,3}^{3,1}\left(\frac{\theta}{\bar{\gamma}_1\bar{\gamma}_2(1-\rho)^2 x}\middle|_{0,\alpha+i,\alpha+i}^{1-\beta,1}\right), \tag{15}$$

where $G_{p,q}^{m,n}[\cdot|\cdot]$ denotes the Meijer's G-function [25, eq. (9.301)]. Note that Meijer's G-function is a standard mathematical function available in many mathematical software packages, e.g., Mathematica, Maple, and thus it can be directly evaluated[2].

In order to study the statistics of Z under favorable, high average SNR conditions, besides (15), we also derive an asymptotic approximation for the CDF of Z which is based on the assumption of high values for the scaling parameters $\bar{\gamma}_j$. With this assumption, using the asymptotic expressions for the modified Bessel functions, i.e., [34, eqs. (03.02.06.0006.01) and (03.04.06.0010.01)], in conjunction with [25, eq. (8.350/1)] and [35, eq. (2.10.3/9)], the CDF of Z is approximated as

$$F_Z(x) \approx \frac{2\left(1+\sqrt{\rho}\right)^{\alpha}}{\Gamma(\alpha)\rho^{\frac{\alpha-1/2}{2}}\Gamma(\beta)} \left\{ \frac{\Gamma\left(\frac{\alpha+1}{2}+\beta\right)}{\alpha+1} g(x)^{\frac{\alpha+1}{2}} \times {}_pF_q\left(\frac{\alpha+1}{2}, \frac{\alpha+1}{2}+\beta; \frac{3}{2}, \frac{\alpha+3}{2}; g(x)^2\right) + \frac{\Gamma(\beta)\Gamma(\alpha)}{2^{\alpha+1}} - \frac{\Gamma\left(\frac{\alpha}{2}+\beta\right)}{2\alpha} g(x)^{\alpha} {}_pF_q\left(\frac{\alpha}{2}+\beta, \frac{\alpha}{2}; \frac{1}{2}, \frac{\alpha+2}{2}; g(x)^2\right) \right\}, \tag{16}$$

where ${}_pF_q(\cdot)$ denotes the generalized hypergeometric function [34, eq. (07.31.02.0001.01)], and $g(x) = \frac{(\theta/x)^{1/2}}{\sqrt{\bar{\gamma}_1\bar{\gamma}_2}(1+\sqrt{\rho})}$. More-

[2]It is noted that a relevant small number of terms in (15), i.e., less than 50, are required in order to achieve an accuracy to the fourth significant decimal digit.

over, for $g(x) \to 0, F_Z(x)$ further simplifies to the following closed-form expression

$$F_Z(x) \approx \frac{2\left(1+\sqrt{\rho}\right)^{\alpha}}{\Gamma(\alpha)\rho^{\frac{\alpha-1/2}{2}}\Gamma(\beta)}\left\{\frac{\Gamma\left(\frac{\alpha+1}{2}+\beta\right)}{\alpha+1}g(x)^{\frac{\alpha+1}{2}} + \frac{\Gamma(\beta)\Gamma(\alpha)}{2^{\alpha+1}} - \frac{\Gamma\left(\frac{\alpha}{2}+\beta\right)}{2\alpha}g(x)^{\alpha}\right\}. \tag{17}$$

Next, we separately study two interesting special cases of this generic model, i.e., the case that shadowing on the S to RIS channel is independent from the RIS to D shadowing, and the case that only one of these two channels is subject to shadowing.

1) Independent shadowing conditions: For independent shadowing conditions, the PDF of L can be evaluated by substituting the expression (12), for the PDF of L, and (7), for the PDF of W, in (11). Then, the following Meijer's G-function representations are exploited

$$\exp(-x) = G_{0,1}^{1,0}\left(x\Big|_{0}^{-}\right), \text{ and } K_v(x) = G_{0,2}^{2,0}\left(\frac{x^2}{4}\Big|_{v/2,v/2}^{-}\right), \tag{18}$$

along with [33, eqs. (11), (21), and (14)]. Moreover, using also [33, eq. (21)] and after some mathematical simplifications, the following exact expressions for the PDF and CDF of Z are finally deduced

$$f_Z(x) = \frac{\theta^{\alpha}/\Gamma(\alpha)^2}{\left(\overline{\gamma}_1\overline{\gamma}_2\right)^{\alpha}\Gamma(\beta)x^{\alpha+1}}G_{1,2}^{2,1}\left(\frac{\theta}{\overline{\gamma}_1\overline{\gamma}_2 x}\Big|_{0,0}^{1-\alpha-\beta}\right) \tag{19}$$

and

$$F_Z(x) = 1 - \frac{\theta^{\alpha}/\Gamma(\alpha)^2}{\left(\overline{\gamma}_1\overline{\gamma}_2\right)^{\alpha}\Gamma(\beta)x^{\alpha}}G_{2,3}^{2,1}\left(\frac{\theta}{\overline{\gamma}_1\overline{\gamma}_2 x}\Big|_{0,0,-\alpha}^{1-\alpha-\beta,1-\alpha}\right). \tag{20}$$

2) Single shadowing scenario: Assuming that shadowing is present in only one of the two links, i.e., either in S-RIS or in RIS-D, the PDF of L is given in (5). Using this PDF in $f_Z(x) = \int_0^{\infty}\frac{1}{y}\tilde{f}_W(y)f_L\left(\frac{x}{y}\right)dy$ and exploiting [25, eqs. (8.310/1), (3.194/2), and (3.194/3)], the following simplified closed-form expressions for the PDF and CDF of Z are obtained

$$f_Z(x) = \frac{\Gamma(\beta+\alpha)}{\theta^{\beta}\Gamma(\beta)\Gamma(\alpha)\overline{\gamma}_1^{\alpha}x^{\alpha+1}}\left(\frac{1}{\theta}+\frac{1}{\overline{\gamma}_1 x}\right)^{-\alpha-\beta}, \tag{21}$$

$$F_Z(x) = \frac{\Gamma(\beta+\alpha)\overline{\gamma}_1^{\beta}x^{\beta}}{\theta^{\beta}\Gamma(\beta)\Gamma(\alpha)\beta}{}_2F_1\left(\beta,\beta+\alpha;\beta+1;-\frac{\overline{\gamma}_1 x}{\theta}\right), \tag{22}$$

where ${}_2F_1(\cdot)$ is the Gauss hypergeometric function [25, eq. (9.100)].

Having determined the PDF and CDF expressions for the RV Z, it is straightforward to obtain the corresponding expressions for the received SNR at D, γ, using a simple scale up by the deterministic factor that is multiplied with Z, i.e., $F_\gamma(\gamma) = F_Z\left(\frac{d_{sr}^v d_{rd}^v}{SNR_T}\gamma\right)$. Having completed the derivation of the PDF and CDF of the SNR, we proceed with the performance analysis of the considered scheme.

C. Performance analysis of the considered scheme

In what follows, we present the performance analysis results which can be obtained with the help of the derived expressions for the PDF of Z and the SNR.

1) Calculation of the outage probability: The OP is defined as the probability that the received SNR is less than a predefined outage threshold $\gamma_{\text{th}} = 2^R - 1$, where R denotes the transmission rate. It can therefore be easily evaluated for all system and channel models under consideration using the CDF expressions derived previously, as

$$P_{\text{out}} = F_\gamma(\gamma_{\text{th}}). \tag{23}$$

2) Calculation of the ergodic capacity: Starting with the definition of the ergodic capacity as $\bar{C} = \mathbb{E}\left[\log_2(1+\gamma)\right]$, we proceed and calculate $\bar{C}$, separately for the independent shadowing and single shadowing scenarios.

a) Independent shadowing: Using (19) and the definition or ergodic capacity, we obtain that its calculation requires the computation of integrals of the form

$$\mathcal{I}_1 = \int_0^{\infty}\frac{\ln(1+x)}{x^{\alpha+1}}G_{1,2}^{2,1}\left(\frac{\theta}{\overline{\gamma}_1\overline{\gamma}_2 x}\Big|_{0,0}^{1-\alpha-\beta}\right)dx. \tag{24}$$

Using the Meijer's G-function representation for the logarithmic function $\ln(1+x) = G_{1,2}^{2,1}\left(x\Big|_{1,0}^{1,1}\right)$, employing a change of variables of the form $x = 1/y$, and applying [25, eq. (9.31/2)] and [33, eq. (21)], integral (24) can be expressed in closed form. Based on this result, the following exact expression for the ergodic capacity can be obtained

$$\bar{C} = \frac{\theta^{\alpha}/[\Gamma(\beta)\ln(2)]}{\left(\overline{\gamma}_1\overline{\gamma}_2\right)^{\alpha}\Gamma(\alpha)^2}G_{3,4}^{3,3}\left(\frac{\theta}{\overline{\gamma}_1\overline{\gamma}_2}\Big|_{0,0,1-\alpha,-\alpha}^{1-\alpha-\beta,1-\alpha,1-\alpha}\right). \tag{25}$$

b) Single shadowing: By substituting (21) in $\bar{C} = \mathbb{E}\left[\log_2(1+\gamma)\right]$, we observe that an integral of the following type appears in the calculation of the ergodic capacity

$$\mathcal{I}_2 = \int_0^{\infty}\frac{\ln(1+x)}{x^{\alpha+1}}\left(\frac{1}{\theta}+\frac{1}{\overline{\gamma}_1 x}\right)^{-\alpha-\beta}dx. \tag{26}$$

This integral can be solved by using the following representation for the Meijer G-function [33, eq. (10)] $\left(\frac{1}{\theta}+\frac{1}{\overline{\gamma}_1 x}\right)^{-\alpha-\beta} = \frac{(\overline{\gamma}_1 x)^{\alpha+\beta}}{\Gamma(\alpha+\beta)}G_{1,1}^{1,1}\left(\frac{\overline{\gamma}_1 x}{\theta}\Big|_{0}^{1-\alpha-\beta}\right)$ and [33, eq. (21)]. Using these expressions and after some mathematical simplifications, the following closed-form expression for the ergodic capacity is derived

$$\bar{C} = \frac{\Gamma(\alpha+\beta)\theta\pi}{\ln(2)\Gamma(\alpha)\Gamma(\beta)\overline{\gamma}_1} \times\left[\left(\frac{\theta}{\overline{\gamma}_1}\right)^{\alpha-1}\frac{\csc(\pi\alpha)}{\alpha}{}_2F_1\left(\alpha,\alpha+\beta;\alpha+1;\frac{\theta}{\overline{\gamma}_1}\right) + \frac{\Gamma(1+\alpha)\Gamma(-1+\beta)}{\pi\Gamma(\alpha+\beta)}{}_pF_q\left(1,1,1+\alpha;2,2-\alpha;\frac{\theta}{\overline{\gamma}_1}\right)\right]. \tag{27}$$

Having derived closed-form expressions for the ergodic capacity of the proposed scheme, we now exploit them in order to study the energy efficiency (EE) characteristics of UAV assisted communications. This is done in what follows.

3) Calculation of the energy efficiency: While adding reflecting elements to an RIS can allow for delivering high-SNR signals at the receiver, in case of airborne RISs, several limitations also need to be considered. In more detail, focusing on small-sized UAVs, their strict battery-capacity constraints should be taken into account, when determining the size of the RIS, expressed in terms of the number of reflecting elements. Motivated by this, in what follows, we discuss the problem of determining the number of reflecting elements, such as to minimize the power consumption of the airborne RIS subject to QoS constraints, expressed in terms of the ergodic capacity.

Therefore, as part of our analysis, we also investigate the average EE of the RIS under consideration. This can be expressed as [36]

$$n_{EE} = BW \frac{\bar{C}}{P_{RIS}}, \tag{28}$$

where BW denotes the bandwidth and P_{RIS} denotes the total power consumption of RIS[3] that can be modeled as [37]

$$P_{RIS} = P_{static} + P_{dynamic}, \tag{29}$$

where P_{static} is the static power consumption and $P_{dynamic}$ is the dynamic power consumption. The latter one depends on the RIS family that has been considered, i.e., varactor-diode-based programmable metasurfaces or PIN-diode-based RIS, in conjunction with their polarization, i.e., vertical, horizontal, or dual. Assuming PIN-diode-based RIS with dual polarization mode, which is twice the single polarization one, as well as one bit resolution, $P_{dynamic}$ can be expressed as

$$P_{dynamic} = 2 \sum_{i=1}^{N} P_{PIN}, \tag{30}$$

where P_{PIN} is the power consumption of the PIN diodes for supporting one bit.

An interesting problem that one can define using the predetermined definition of EE is the one of determining the number of phase shifters that should be present on an airborne RIS such as to maximize the EE subject to a target ergodic capacity constraint. This is expressed as follows

$$\begin{aligned} &\max_{M} \; n_{EE} \\ &\text{s.t.} \; \mathrm{BW}\, \bar{\mathrm{C}}(\mathrm{P_S}, \mathrm{M}) \geq \mathrm{c}^*, \mathrm{P_S} > 0, \mathrm{M} > 0, \end{aligned} \tag{31}$$

where c^* denotes a capacity target, while P_S is considered to be fixed.

V. Numerical Results

In this section, we utilize our new analytical expressions along with corresponding ones obtained by means of Monte Carlo simulations (using 10^6 samples) such as to analyze the performance of the considered system. If not otherwise stated, the parameters used in our analysis are included in Table I and their values are very common in various measurement campaign-based studies in this area [20][4]. It is noted the values of these parameters correspond to open field ($v = 2.2$), line-of-sight ($k = 2$) propagation conditions with light shadowing ($\alpha = 2$). Moreover, without loosing the generality of our results, in most scenarios examined, the UAV is assumed to be located at the middle of the S-D distance. Finally, for comparison purposes, we also investigate the behavior of a system setup, in which the S communicates to the D with the aid of a single-antenna relay that is mounted on a UAV. To this aim, two protocols have been studied, namely, the Full-Duplex Decode-and-Forward (FDDF) and the Half-Duplex Decode-and-Forward (HDDF). The later one requires two orthogonal channels to be available for forwarding the information from the S to the D. Details regarding the analytical statistical metrics of these benchmarks can be found in the Appendix.

TABLE I: Simulation parameters definition and values.

Parameter	Definition	Value
v	Path loss factor	2.2
P_S	S transmit power	-5dBm
N_0	Noise power	-97.8dBm
h	UAV height	60m
r_{tot}	Total S-D distance	200m
M	Number of reflecting elements	16
k	Weibull shaping parameter	2
α	IG shaping parameter	2

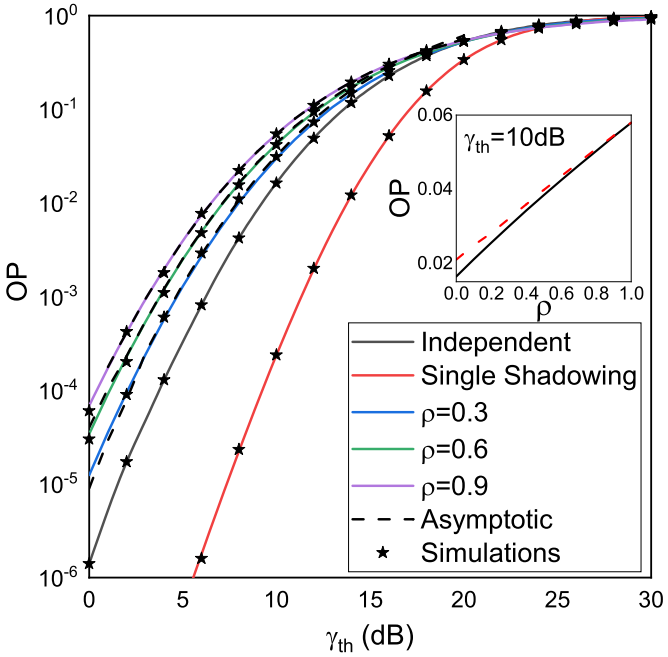

Fig. 3: OP vs outage threshold (with shadowing correlation as a parameter of interest).

In Fig. 3, based on (15), (20), and (22), the OP is plotted as a function of the outage threshold γ_{th} for different shad-

[3]It is noted that the current investigation explicitly focuses on the power consumption of the RIS. If other parameters are also taken into account at the power modeling, e.g., the power consumed for hovering, transiting, a different approach should be followed similar to the one proposed in [16].

[4]Most of these values are based on a channel measurement campaign of UAV-to-ground links at both 2.4 and 5 GHz bands [38].

This article has been accepted for publication in IEEE Transactions on Vehicular Technology. This is the author's version which has not been fully edited and content may change prior to final publication. Citation information: DOI 10.1109/TVT.2024.3364383

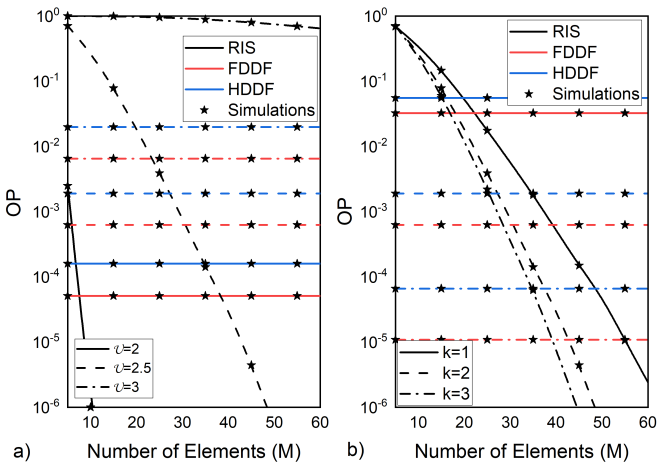

Fig. 4: OP vs the number of elements M (with path loss factor and multipath fading severity as parameters of interest).

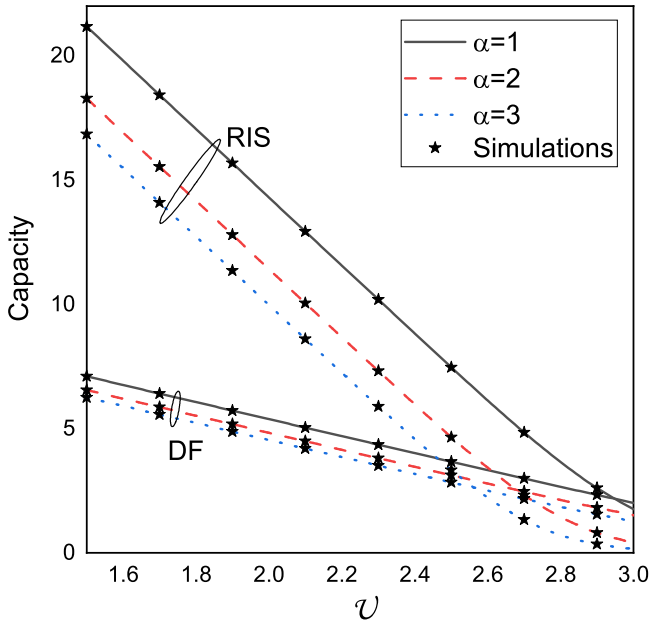

Fig. 5: Capacity vs path loss factor (with shadowing severity as a parameter of interest).

owing environments, including correlated, independent, and single shadowing scenarios. Interestingly, the results of Fig. 3 show that the performance deteriorates as the shadowing correlation increases. This can be explained by the fact that in the extreme scenario, where independent shadowing is assumed, the probability of both (S-UAV and UAV-D) links to suffer from deep shadowing is small and thus scenarios with severe shadowing in both links do not appear very often. This situation changes if correlation between shadowing in the two areas is present, since in that case, deep shadowing can occur in both links. It is also noted that for lower values of the outage threshold $\gamma_{\rm th}$, the OP doubles as the correlation coefficient tends from 0.3 to 0.6. However, this behavior is not observed for higher values of $\gamma_{\rm th}$. Moreover, we clearly see the considerable performance improvement induced in cases where shadowing is only present in one of the two regions. Finally, in the same figure, using (16), the asymptotic OP is also plotted proving that in all cases it is an excellent, low complexity approximation to the exact OP value. It is interesting to note that this approximation improves as the correlation coefficient increases, as it is more clearly depicted in the small graph included in Fig. 3.

In Fig. 4.a, the impact of path loss factor and Weibull shaping parameter to the OP performance is studied. The results in Fig. 4 also consider two benchmark scenarios: a) a HDDF scheme, where the UAV is equipped with a single antenna and supports a pure HDDF protocol and b) an idealistic FDDF scheme, in which reception and transmission from the S to D occur concurrently and at the same frequency, while the relay does not suffer from any self-interference. The OP of FDDF is also based on (32), with $\gamma_{\rm th} = 2^R - 1$[5]. It is obvious that the performance of FDDF is clearly unachievable and thus it can be considered as an upper bound of the HDDF. We observe that for lower values of v, the performance of RIS-assisted communication is of the order of magnitude better as compared to the other cases, even for very small number of the RIS elements. As v increases, more elements are required in order to achieve better performance to the traditional communication techniques. Moreover, Fig. 4.b depicts that the performance improves as the fading conditions get better, i.e., as k increases. Finally, in the latter subfigure, it is also shown that for worse small-scale fading conditions, a smaller number of elements M is required in order to achieve better performance. In Fig. 5, using (25) and (27), the ergodic channel capacity is investigated in conjunction with the path loss factor for RIS and HDDF-assisted UAV communications (with $M = 64$). In this figure, it is shown that the capacity decreases as the path loss factor (v) increases and/or the severity of the shadowing (that is controlled by the shaping parameter α) also increases. It is interesting to be noted that for smaller values of v, which usually appear in UAV-aided communications, the performance of RIS-assisted communications is much better than that of HDDF. However, the performance of the RIS scheme highly depends on the variations of the path loss factor, since as $v \to 3$ its performance is almost 20 times smaller as compared to the corresponding one for lower values of v. Finally, it is worth-noting that in Figs. 3-5, an excellent agreement is observed between the simulated and the analytical results.

In Fig. 6, focusing on the independent shadowing scenario using (25), the capacity is plotted as a function of the UAV height and the normalized distance, defined as $\Lambda = \frac{r_1}{r_{tot}}$, where r_1 is the S-UAV ground distance. A general comment is that a symmetry in the capacity performance is observed with respect to the normalized distance of the UAV, between the S and D. Moreover, it is shown that the performance deteriorates with the increase of the UAV height, since in that case the total distance also increases. It is interesting to note that for lower UAV heights, i.e., h being around 40m, the maximum value of the capacity can be obtained in the

[5]It is noted that for the HDDF relaying protocol, the outage threshold is given by $\gamma_{\rm th} = 2^{2R} - 1$.

This article has been accepted for publication in IEEE Transactions on Vehicular Technology. This is the author's version which has not been fully edited and content may change prior to final publication. Citation information: DOI 10.1109/TVT.2024.3364383

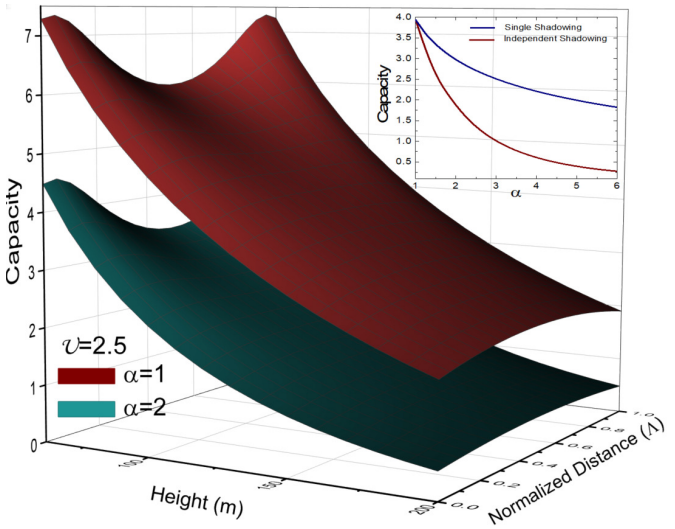

Fig. 6: Capacity vs UAV height and S-D normalized distance (with shadowing severity as a parameter of interest).

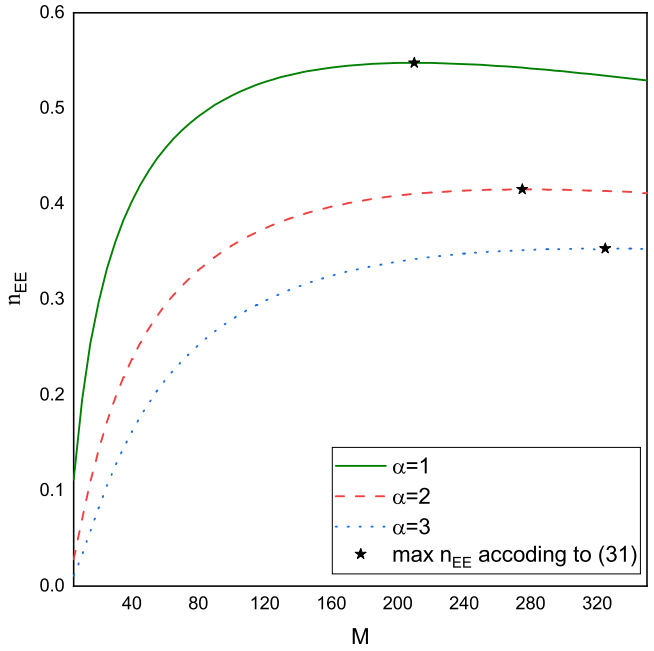

Fig. 7: Energy efficiency vs the number of reflecting elements M (with shadowing severity as a parameter of interest).

limiting regions when $\Lambda \to 0$ or $\Lambda \to 1$, while for higher values of h, the maximum value is obtained when the UAV is located at the middle of the distance between the S and D. The same observation holds for both assumptions of the shadowing severity. Moreover, it is also shown that higher values of α result to more severe shadowing. This is also confirmed by the small graph included in Fig. 6, where an exponential decrease of the capacity is observed as shadowing parameter α increases under both shadowing scenarios, namely single shadowing and independent shadowing. From this small graph is it also noted that the performance is always better is single shadowing scenario especially for larger values of α.

In Fig. 7, the average EE is plotted as a function of the number of reflecting elements for different (independent) shadowing conditions[6]. Based on the results presented in [37], a dual-polarized RIS is assumed that belongs to the family of PIN-diode based programmable metasurfaces, whose operating frequency is at $f = 35$ GHz. Regarding the RIS dimensions, the total length and width are 0.228 m $\times$ 0.228 m, and it is composed of 60×60 reduplicated unit cells. To obtain this figure, the following parameters have been employed: $r_1 = r_2$, $h = 100$m, $v = 2.5$, $P_{static} = 15.73$W, $P_{PIN} = 12.6$mW. In this figure, it is shown that for small to moderate values of M, i.e., $10 \leq M \leq 60$, the EE performance is rapidly increasing as M increases. However, this behavior is not observed for higher values of M. In all cases the most efficient performance is obtained when light shadowing conditions are assumed, i.e., $\alpha = 1$. It is also noted that the EE reaches a maximum value that corresponds to the optimization solution that has been numerically evaluated in (31), assuming that the normalized channel capacity is equal to 2. After that point the EE gradually decreases as M increases. Therefore, from the results presented in Fig. 7, it is evident that in all scenarios with a very small penalty on the achieved EE performance, e.g., 5%, the required number of RIS elements can be reduced to one half of that of the maximum value. This observation is very important in UAV-assisted communication scenarios, since the number of reflecting elements is directly related to the UAV weight and as a result to its flight duration.

[6]It is noted that RIS-assisted communication systems have, in general, better EE performance as compared to the decode-and-forward ones [36] and thus in this study such a comparison has been omitted.

VI. Conclusions

In this paper, the impact of correlated shadowing on an aerial-RIS wireless communication system was analytically investigated. More specifically, an analytical tool for evaluating important stochastic performance metrics of the received SNR was presented, which uses easy-to-evaluate expressions. Moreover, highly accurate asymptotic results have been also obtained that greatly simplify the numerical evaluation of the performance metrics under investigation. In the presented numerical results, it was for the first time depicted that shadowing correlation has a notable impact to the system's performance, while under various scenarios, the performance of the scheme under investigation is much better than traditional, cooperative relaying scenarios. Moreover, based on the results presented, it was shown that even with a small number of reflecting elements, an excellent performance is achieved, in terms of capacity and energy efficiency. Finally, we briefly outline that concerning possible extensions of our work, several open challenges exist, with the most notable being the relaxation of the assumption of ideal CSI and phase correction.

Appendix
Decode-and-Forward Analysis

In this appendix, analytical results for a decode-and-forward (DF) aerial cooperative communication scenario are presented. In this context it is assumed that a S communicates to the D

with the aid of a single antenna DF aerial relay. In that case, the CDF of the E2E received SNR at the D is then expressed as [39]

$$F_{\gamma_{DF}}(x) = 1 - \left(1 - F_{\gamma_{sr}}(x)\right)\left(1 - F_{\gamma_{rd}}(x)\right), \tag{32}$$

where

$$\gamma_{sr} = \frac{P_S}{N_0 d_{sr}^v}|w_1 L_1|, \gamma_{rd} = \frac{P_S}{N_0 d_{rd}^v}|w_2 L_2|. \tag{33}$$

Focusing on the independent shadowing scenario, using CDF expressions of the form presented in (22) in (32) and after some mathematical manipulations, the CDF of γ_{DF} can be expressed in the following closed-form expression

$$\begin{aligned} F_{\gamma_{DF}}(x) =& 1 - \prod_{i=1}^{2}\left[1 - \frac{(\overline{\gamma}_i x)^\beta}{\Gamma(\alpha)}\frac{\Gamma(\alpha+\beta)}{\Gamma(\beta)}\right. \\ & \left. \times\ {}_2F_1\left(\beta, \alpha+\beta; 1+\beta; -\frac{\overline{\gamma}_i x}{\theta}\right)\right]. \end{aligned} \tag{34}$$

It is noted that to the best of the authors' knowledge, (34) is the first time that has been reported in the open technical literature. Moreover, in order to investigate the capacity of such a system, (34) has been employed in the following expression $\bar{C} = \frac{BW}{\ln 2}\int_0^\infty \frac{1-F_{\gamma_{DF}}(x)}{1+x}dx$. The value of this integral can be easily approximated by employing the Gauss–Laguerre quadrature method [32].

REFERENCES

[1] M. A. ElMossallamy, H. Zhang, L. Song, K. G. Seddik, Z. Han, and G. Y. Li, "Reconfigurable intelligent surfaces for wireless communications: Principles, challenges, and opportunities," *IEEE Trans. Cogn. Commun. Netw.*, vol. 6, no. 3, pp. 990–1002, 2020.

[2] E. Basar, M. Di Renzo, J. De Rosny, M. Debbah, M.-S. Alouini, and R. Zhang, "Wireless communications through reconfigurable intelligent surfaces," *IEEE Access*, vol. 7, pp. 116 753–116 773, 2019.

[3] D. Tyrovolas, S. A. Tegos, E. C. Dimitriadou-Panidou, P. D. Diamantoulakis, C. K. Liaskos, and G. K. Karagiannidis, "Performance analysis of cascaded reconfigurable intelligent surface networks," *IEEE Wireless Commun. Lett.*, vol. 11, no. 9, pp. 1855–1859, 2022.

[4] L.-C. Wang, H. Peng, A. C.-S. Huang, and A.-H. Tsai, "Latest advances in spectrum management for 6G communications," in *30th Wireless and Optical Communications Conference (WOCC)*, 2021, pp. 295–297.

[5] D. Tyrovolas, S. A. Tegos, P. D. Diamantoulakis, and G. K. Karagiannidis, "Synergetic UAV-RIS communication with highly directional transmission," *IEEE Wireless Commun. Lett.*, vol. 11, no. 3, pp. 583–587, 2022.

[6] L. Yang, F. Meng, J. Zhang, M. O. Hasna, and M. D. Renzo, "On the performance of RIS-assisted dual-hop UAV communication systems," *IEEE Trans. Veh. Technol.*, vol. 69, no. 9, pp. 10 385–10 390, 2020.

[7] L. Yang, P. Li, F. Meng, and S. Yu, "Performance analysis of RIS-assisted UAV communication systems," *IEEE Trans. Veh. Technol.*, vol. 71, no. 8, pp. 9078–9082, 2022.

[8] X. Liu, Y. Liu, and Y. Chen, "Machine learning empowered trajectory and passive beamforming design in UAV-RIS wireless networks," *IEEE J. Sel. Areas Commun.*, vol. 39, no. 7, pp. 2042–2055, 2021.

[9] C. Xu *et al.*, "Reconfigurable intelligent surface assisted multi-carrier wireless systems for doubly selective high-mobility ricean channels," *IEEE Trans. Veh. Technol.*, vol. 71, no. 4, pp. 4023–4041, 2022.

[10] N. Agrawal, A. Bansal, K. Singh, and C.-P. Li, "Performance evaluation of RIS-assisted UAV-enabled vehicular communication system with multiple non-identical interferers," *IEEE Trans. Intell. Transp. Syst.*, vol. 23, no. 7, pp. 9883–9894, 2022.

[11] T. V. Nguyen, H. D. Le, and A. T. Pham, "On the design of RIS-UAV relay-assisted hybrid FSO/RF satellite-aerial-ground integrated network," *IEEE Aerosp. Electron. Syst. Mag.*, pp. 1–15, 2022.

[12] T. N. Do, G. Kaddoum, T. L. Nguyen, D. B. da Costa, and Z. J. Haas, "Aerial reconfigurable intelligent surface-aided wireless communication systems," in *IEEE Annual Int. Symposium on Personal, Indoor and Mobile Radio Commun. (PIMRC)*, 2021, pp. 525–530.

[13] A. Bhowal and S. Aïssa, "RIS-aided communications in indoor and outdoor environments: Performance analysis with a realistic channel model," *IEEE Trans. Veh. Technol.*, vol. 71, no. 12, pp. 13 356–13 360, 2022.

[14] N. P. Le *et al.*, "Energy-harvesting aided unmanned aerial vehicles for reliable ground user localization and communications under lognormal-nakagami-m fading channels," *IEEE Trans. Veh. Technol.*, vol. 70, no. 2, pp. 1632–1647, 2021.

[15] N. Bhargav, C. R. N. da Silva, Y. J. Chun, E. J. Leonardo, S. L. Cotton, and M. D. Yacoub, "On the product of two $\kappa-\mu$ random variables and its application to double and composite fading channels," *IEEE Trans. Wireless Commun.*, vol. 17, no. 4, pp. 2457–2470, 2018.

[16] D. Tyrovolas, P.-V. Mekikis, S. A. Tegos, P. D. Diamantoulakis, C. K. Liaskos, and G. K. Karagiannidis, "Energy-aware design of UAV-mounted RIS networks for IoT data collection," *IEEE Trans. Commun.*, vol. 71, no. 2, pp. 1168–1178, 2022.

[17] S. Atapattu, R. Fan, P. Dharmawansa, G. Wang, J. Evans, and T. A. Tsiftsis, "Reconfigurable intelligent surface assisted two–way communications: Performance analysis and optimization," *IEEE Trans. Wireless Commun.*, vol. 68, no. 10, pp. 6552–6567, 2020.

[18] J. He, W. Cheng, Z. Tang, D. López-Pérez, and H. Claussen, "Analytical evaluation of higher order sectorization, frequency reuse, and user classification methods in OFDMA networks," *IEEE Trans. Wireless Commun.*, vol. 15, no. 12, pp. 8209–8222, 2016.

[19] D. W. Matolak, "Unmanned aerial vehicles: Communications challenges and future aerial networking," in *Int. Conf. on Comput., Netw. and Commun. (ICNC)*, 2015, pp. 567–572.

[20] A. A. Khuwaja, Y. Chen, N. Zhao, M. Alouini, and P. Dobbins, "A survey of channel modeling for UAV communications," *IEEE Commun. Surv. Tutor.*, vol. 20, no. 4, pp. 2804–2821, 2018.

[21] T. Li *et al.*, "Secure UAV-to-vehicle communications," *IEEE Trans. Commun.*, vol. 69, no. 8, pp. 5381–5393, 2021.

[22] J. Reig, M.-T. Martínez-Inglés, L. Rubio, V.-M. Rodrigo-Penarrocha, and J.-M. Molina-García-Pardo, "Fading evaluation in the 60 Ghz band in line-of-sight conditions," *International Journal of Antennas and Propagation*, vol. 2014, 2014.

[23] P. S. Bithas, G. K. Karagiannidis, N. C. Sagias, P. T. Mathiopoulos, S. A. Kotsopoulos, and G. E. Corazza, "Performance analysis of a class of GSC receivers over nonidentical Weibull fading channels," *IEEE Trans. Veh. Technol.*, vol. 54, no. 6, pp. 1963–1970, 2005.

[24] P. S. Bithas, V. Nikolaidis, A. G. Kanatas, and G. K. Karagiannidis, "UAV-to-ground communications: Channel modeling and UAV selection," *IEEE Trans. Commun.*, vol. 68, no. 8, pp. 5135–5144, Aug. 2020.

[25] I. S. Gradshteyn and I. M. Ryzhik, *Table of Integrals, Series, and Products*, 6th ed. New York: Academic Press, 2000.

[26] G. L. Stüber, *Principles of mobile communication*. Springer Science & Business Media, 2011.

[27] N. P. Le *et al.*, "Energy-harvesting aided unmanned aerial vehicles for reliable ground user localization and communications under lognormal-nakagami-m fading channels," *IEEE Trans. Veh. Technol.*, vol. 70, no. 2, pp. 1632–1647, 2021.

[28] P. S. Bithas, A. G. Kanatas, and D. W. Matolak, "Exploiting shadowing stationarity for antenna selection in V2V communications," *IEEE Trans. Veh. Technol.*, vol. 68, no. 2, pp. 1607–1615, Feb 2019.

[29] S. Al-Ahmadi and H. Yanikomeroglu, "On the approximation of the generalized-k distribution by a gamma distribution for modeling composite fading channels," *IEEE Trans. Wireless Commun.*, vol. 9, no. 2, pp. 706–713, 2010.

[30] L. Devroye, *Non-Uniform Random Variate Generation*. Springer, New York, NY, 1986.

[31] A. Papoulis and S. Pillai, *Probability, Random Variables, and Stochastic Processes*, 4th ed. New York: McGraw-Hill, 2002.

[32] M. Abramowitz and I. A. Stegun, *Handbook of mathematical functions: with formulas, graphs, and mathematical tables*. Courier Corporation, 1964, vol. 55.

[33] V. S. Adamchik and O. I. Marichev, "The algorithm for calculating integrals of hypergeometric type functions and its realization in REDUCE system," in *Proc. Int. Conf. on Symbolic and Algebraic Computation*, Tokyo, Japan, 1990, pp. 212–224.

[34] The Wolfram Functions Site, 2023. [Online]. Available: http://functions.wolfram.com

[35] A. Prudnikov, Y. Brychkov, and O. Marichev, *Integrals and Series, Vol. 2*. Gordon and Breach Science Publishers, 1986.

[36] C. Huang, A. Zappone, G. C. Alexandropoulos, M. Debbah, and C. Yuen, "Reconfigurable intelligent surfaces for energy efficiency in wireless communication," *IEEE Trans. Wireless Commun.*, vol. 18, no. 8, pp. 4157–4170, 2019.

[37] J. Wang *et al.*, "Reconfigurable intelligent surface: Power consumption modeling and practical measurement validation," *arXiv preprint arXiv:2211.00323*, 2022.
[38] E. Yanmaz, R. Kuschnig, and C. Bettstetter, "Channel measurements over 802.11a-based UAV-to-ground links," in *IEEE GLOBECOM Workshops (GC Wkshps)*. IEEE, 2011, pp. 1280–1284.
[39] S. Zeng, H. Zhang, K. Bian, and L. Song, "UAV relaying: Power allocation and trajectory optimization using decode-and-forward protocol," in *IEEE Intern. Conf. on Commun. (ICC Workshops)*, 2018, pp. 1–6.

Petros S. Bithas (S'04-M'09-SM'19) received the Diploma in electrical and computer engineering and PhD degree, from the University of Patras, Greece, in 2003 and 2009, respectively. From 2010 to 2020, he was an associate researcher at the Department of Digital Systems, University of Piraeus, Greece, where he was involved in various National and European Research and Development projects. He is currently an Associate Professor at the Department of Digital Industry Technologies of the National & Kapodistrian University of Athens, Greece. Prof. Bithas has authored or co-authored more than 100 Journal and Conference papers and 2 Book chapters. He acts as Associate Editor for 5 international scientific Journals, including `IEEE Communication Letters`. His research interests are in the areas of wireless communications and optical communications systems.

George A. Ropokis is an Associate Professor at CentraleSupélec, Campus Rennes, also affiliated with the Institute of Electronics and Telecommunications of Rennes. He received the Diploma degree in Computer Engineering and Informatics from the Univ. of Patras, Greece in 2004, the M.Sc. degree in Mobile and Satellite Communications from the Univ. of Surrey, U.K. and the Ph.D. degree in Wireless Communications from the Univ. of Patras in 2010. From 2012 to 2014 he was a Visiting Scientist at the Mobile Comm. Dept., EURECOM, France. From 2016 to 2018, he served as a Research Fellow at CONNECT centre, Trinity College Dublin, Ireland. His research interests are focused on the performance analysis and optimization of Wireless Communications systems.

George K. Karagiannidis (M'96-SM'03-F'14) is currently Professor in the Electrical and Computer Engineering Dept. of Aristotle University of Thessaloniki, Greece and Head of Wireless Communications Lamp and Information Processing (WCIP) Group. He is also Faculty Fellow in the Artificial Intelligence & Cyber Systems Research Center, Lebanese American University. His research interests are in the areas of Wireless Communications Systems and Networks, Signal Processing, Optical Wireless Communications, Wireless Power Transfer and Applications and Communications, Signal Processing for Biomedical Engineering. Dr. Karagiannidis is the Editor-in Chief of `IEEE Transactions on Communications` and in the past was the Editor-in Chief of `IEEE Communications Letters`. Recently, he received three prestigious awards: The 2021 IEEE ComSoc RCC Technical Recognition Award, the 2018 IEEE ComSoc SPCE Technical Recognition Award and the 2022 Humboldt Research Award from Alexander von Humboldt Foundation. Dr. Karagiannidis is one of the highly-cited authors across all areas of Electrical Engineering, recognized from Clarivate Analytics as Web-of-Science Highly-Cited Researcher in the nine consecutive years 2015-2023.

Hector E. Nistazakis (BSc 1997, MSc 1999, PhD 2002), was born in Athens, Greece. He is a Professor of Electronic Physics, Head of the Department of Physics of the National Kapodistrian University of Athens and Director of the Laboratory of Physics. Prof. Nistazakis has authored or co-authored more than 270 Journal and Conference papers, 13 Book chapters and 3 Books. He acts as Associate or Guest Editor for 8 international scientific Journals, as TPC member for more than 30 international conferences and as organizing committee in 5 conferences. His current research interests include topics as optical communication systems, wireless communications, FSO links, UOWC systems, VLC, nonlinear dynamics, analog and digital circuits and systems, nonlinear circuits and systems and computational methods in telecommunications and physics.